Electronic Supplementary Material (ESI) for Physical Chemistry Chemical Physics.

Supporting Information

Probing Acid Sites in Solid Catalysts with Pyridine UV-Vis Spectroscopy

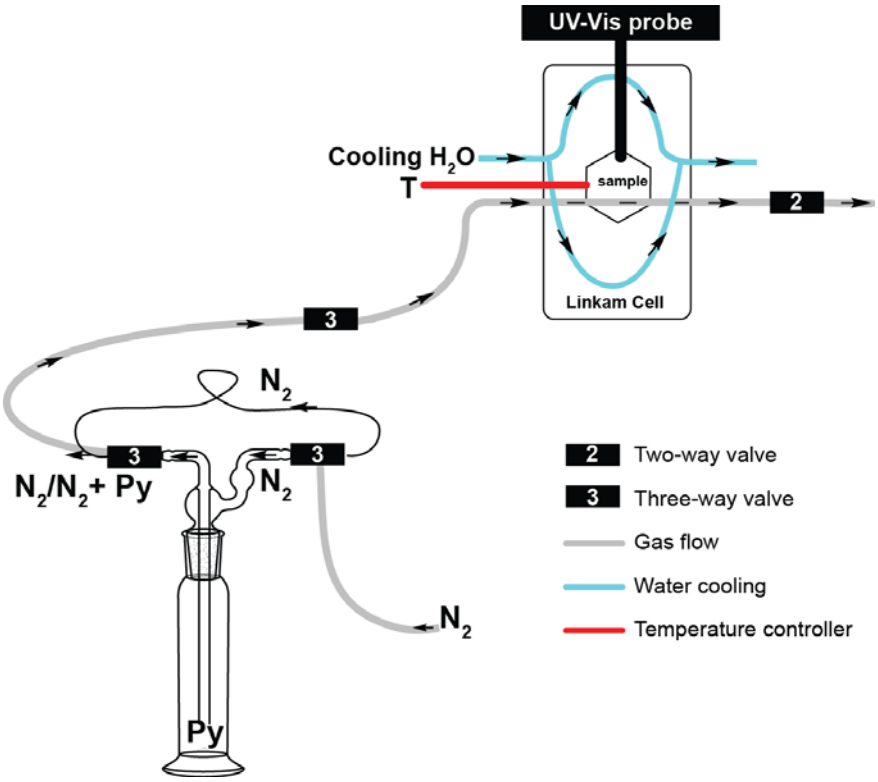

Scheme S1: Designed setup for the pyridine UV-Vis diffuse reflectance spectroscopy experiments. The N_2 flows through a pyridine saturator prior to entering the Linkam cell. In the cell, the sample can be heated with a temperature controller, while the rest of the cell can be kept at RT with cooling water. The adsorption and consequent desorption of pyridine is followed with a UV-Vis probe.

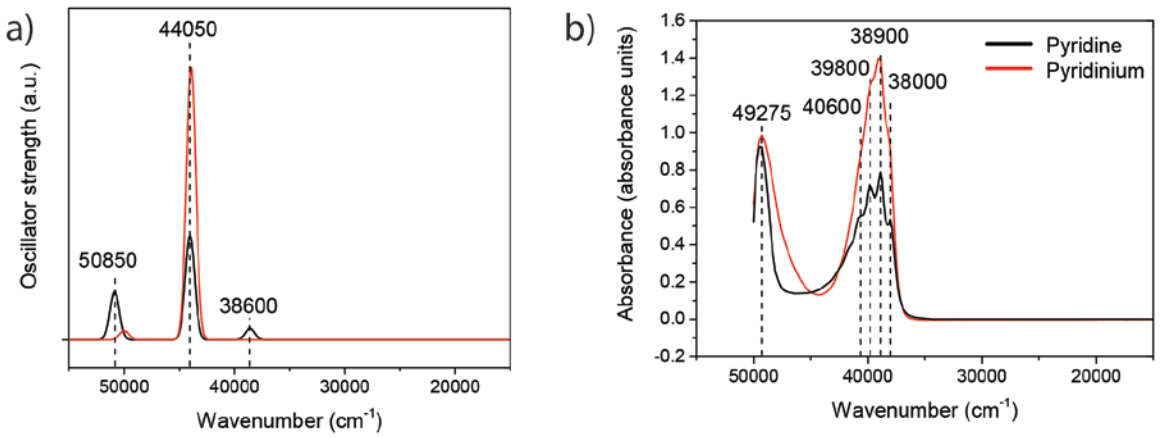

Figure S1: Experimental UV-Vis absorption spectra of pyridine and pyridinium. Calculated excitation energies are broadened with a Gaussian function with a peak width of 1000 cm^{-1}. Experimental spectra were collected of 0.0005 M pyridine and pyridinium in ethanol.

The experimental UV-Vis absorption spectra were collected with a Varian Cary 500 UV-vis-NIR spectrometer against a pure ethanol reference standard. Spectra were collected between 800-200 nm with a data interval of 1 nm. Calculations (simulations) were done with Amsterdam Density Functional (ADF) 2016.[1,2] Geometry optimizations *for pyridine and pyridinium* were performed with the B3LYP functional and the TZP basis set. The first twenty allowed Davidson excitation energies were calculated for the geometrically optimized structures with the same settings.

In the experimental spectra, two absorption maxima are observed at 38900 and 49275 cm^{-1} for pyridine. These bands are assigned to the HOMO-LUMO and HOMO-LUMO+1 excitation within the π-system of pyridine, respectively, and correspond to the bands at 44050 and 50850 cm^{-1} in the simulated spectra. The differences in energy are due to systematic errors with respect to the energy of the TD-DFT calculations. Pyridinium shows the same absorption bands, although slightly redshifted and more intense. The sharp peaks on top of the band at 38900 cm^{-1} in the experimental spectrum are assigned to the coupling with the vibronic spectrum of the pyridine molecule. Furthermore, the TD-DFT calculations indicate that the peak lowest in energy (38600 cm^{-1}) belongs to a n-π* transition. The non-bonding electrons originate from the lone pair on the nitrogen and do not participate in the conjugated π-system. A n-π* transition within the pyridine molecule is forbidden, so this could be an explanation why this transition is too weak to be observed in the experimental spectrum of pyridine. In pyridinium, these electrons bind the proton, and therefore, lose their non-bonding character.

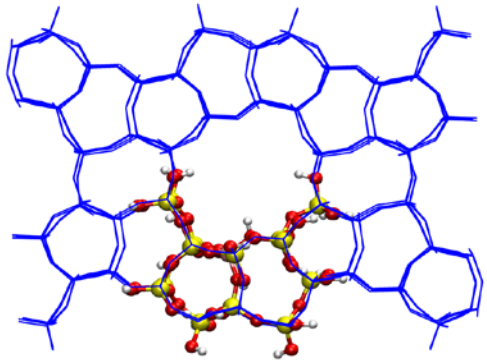

Next, the adsorption of pyridine on a Brønsted acid site and a Lewis acid site, including the resulting electronic spectrum was modeled. To that end, a ZSM-5 cluster of 85 atoms with an active site on the T3 position (intersection) was created from periodic MFI structures taken from the IZA-database, as shown in Figure S2. Terminal oxygen atoms of the cluster were protonated and the structure was optimized using a BLYP functional and a TZP basis set.

Figure S2: The cluster model of a ZSM-5 zeolite.

Pyridine on BAS: Next, a pyridine molecule was adsorbed on the modeled Brønsted acid site and the structure was re-optimized. After the optimization, the N-H distance was found 1.06 Å, while the O(framework)-H distance increased to 1.67Å. This indicates the Brønsted basic character of the pyridine, which forms pyridinium and remains adsorbed on the active site. After geometry optimization, the UV-Vis spectra were computed using a B3LYP functional with a TZ2P basis set.

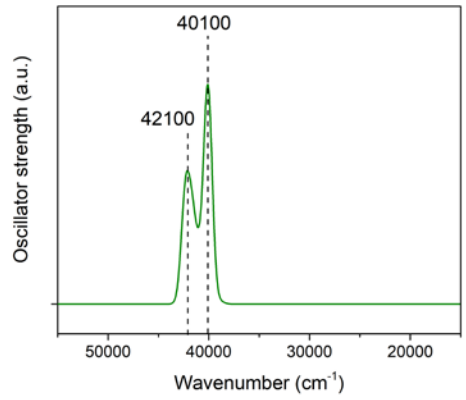

Figure S3: Computed UV-Vis spectrum of pyridinium adsorbed on the active site in a zeolite cluster. Calculated excitation energies are broadened with a Gaussian function with a peak width of 1000 cm^{-1}.

When strongly coordinated to the active site within the zeolite cluster, the adsorption spectrum of pyridinium changes significantly compared to its vacuum spectrum (Figure S1a). Figure S3 shows that multiple peaks appear in UV-VIS region, which are red-shifted significantly (±4000 cm^{-1}). Moreover, contrary to gas phase calculations, all peaks in this region correspond to n-π* transitions. The π-π* excitation within the pyridinium does not occur anymore. This demonstrates that upon interaction with the surface, the electronic properties of the pyridine alter significantly through complexation with the solid acid. All excitations that take place in the UV-Vis region occur through charge transfers within the pyridine-zeolite complex. The most intense peak in Figure S3 at 40100 cm^{-1} is caused by a charge transfer from the zeolitic complex to the LUMO of the pyridine molecule, a s illustrated in Figure S4.

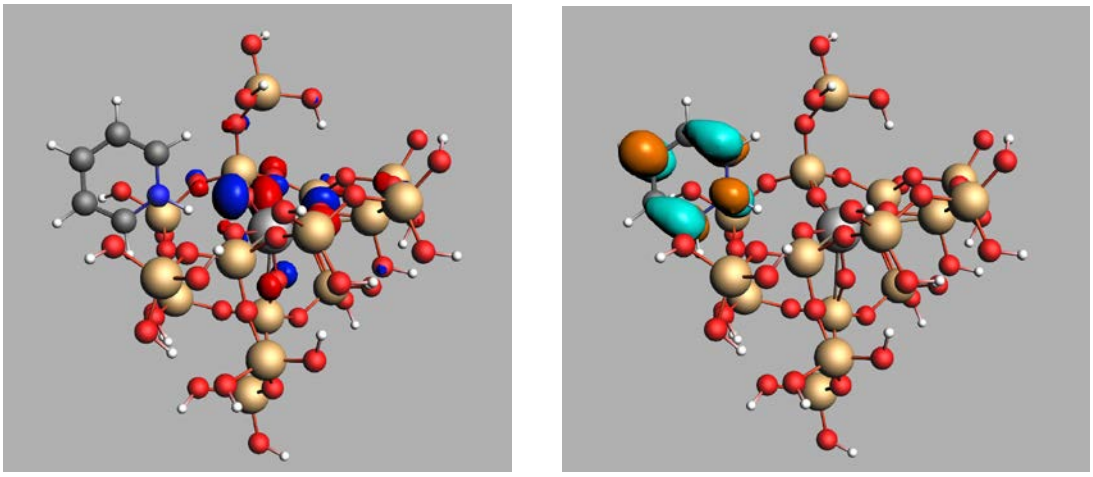

Figure S4: n- π* transition corresponding to the excitation at 40100 cm^{-1}. This is a charge transfer from the zeolitic framework to the LUMO of the pyridinium molecule.

Pyridine on LAS: In order to simulate (weak) Lewis acid sites in the same zeolitic framework, the proton at the active site, causing the Brønsted acidic character, was replaced by a Na cation. This structure was re-optimized first, prior to introducing a pyridine molecule to this system. This pyridine-Na-zeolite complex was again re-optimized. After this second geometry optimization, the pyridine was found to be weakly coordinated on LAS with a N-Na distance of 2.5 Å. After geometry optimization, this UV-Vis spectrum was also computed using a B3LYP functional with a TZ2P basis set.

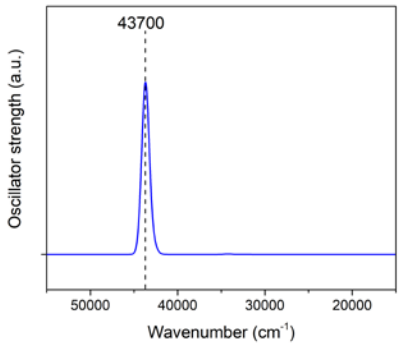

Figure S5: Computed UV-Vis spectrum of pyridinium adsorbed on the active site in a zeolite cluster. Calculated excitation energies are broadened with a Gaussian function with a peak width of 1000 cm^{-1}.

The computed spectrum for the pyridine-Na-zeolite complex is depicted in Figure S5. The strongest excitation occurs at 43700 cm^{-1}, corresponding to the π–π* transition within the pyridine molecule. Compared to the gas phase calculations, the position of this π–π* excitation is negligibly red-shifted (about 350 cm^{-1}). The (much weaker and not shown) n- π* transition peak now appears at 42850 cm^{-1}, corresponding to a red-shift of 4250 cm^{-1}. This excitation is depicted in Figure S6. The shift compared with the gas phase pyridine molecule is more than 10 times larger than the shift for the π - π* transition. This means that the pyridine molecule and its conjugated system remains intact and only the lone pair on the nitrogen is significantly influenced. Interesting to note that charge transfers from the zeolite framework to the pyridine do not take place. This is caused by the considerable distance between the pyridine molecule and the zeolite-Na framework. In the case of the pyridine-BAS framework, the orbitals from both sides could overlap and charge transfers could take place. Compensating cations such as Na+ or K+ are large and considered weak Lewis acid sites. One might speculate, that when adsorbed on stronger LAS, such as Al cations, the N-Al bond length will be smaller and orbital lap can occur, leading to charge transfers, shifting the absorption energies.

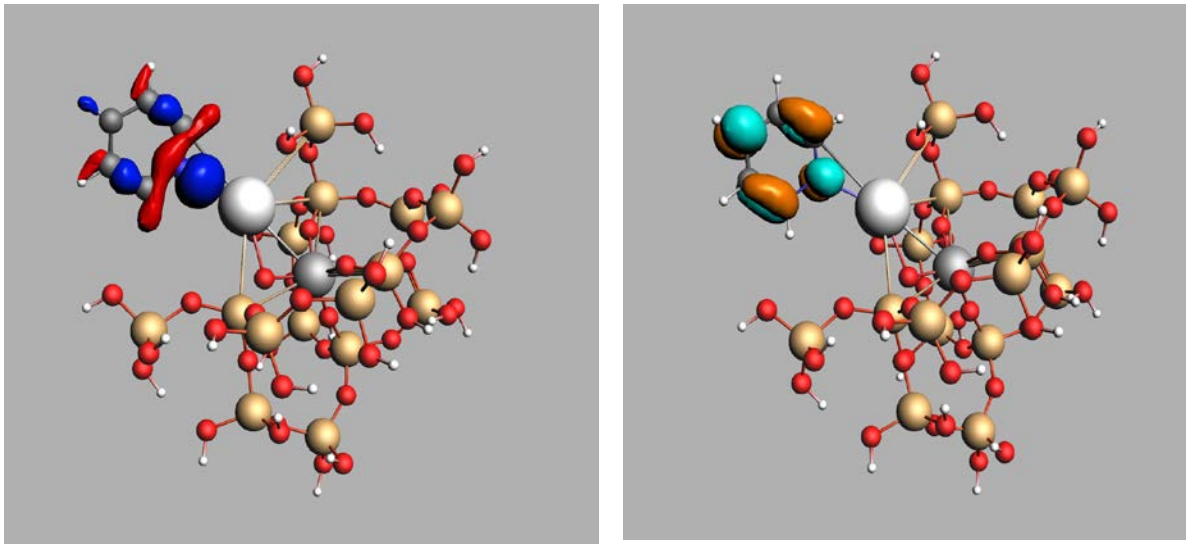

Figure S6: The n- π* transition corresponding to the excitation at 40 084 cm^{-1} for the pyridine-Na-zeolite complex: A charge transfer from nitrogen atom to the LUMO orbital of pyridine takes place.

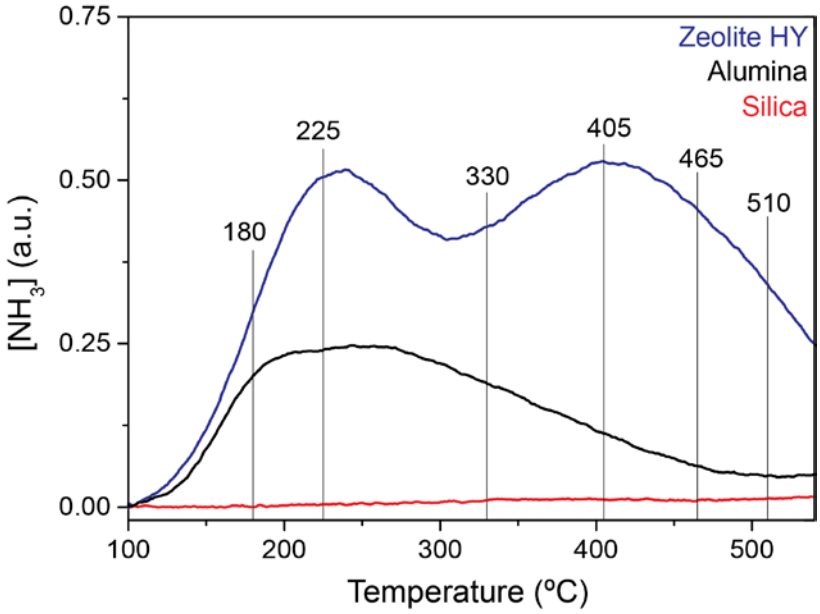

Figure S7: NH_3-TPD profiles versus temperature for the three reference samples Zeolite H-Y (blue), Alumina (black), and Silica (red).

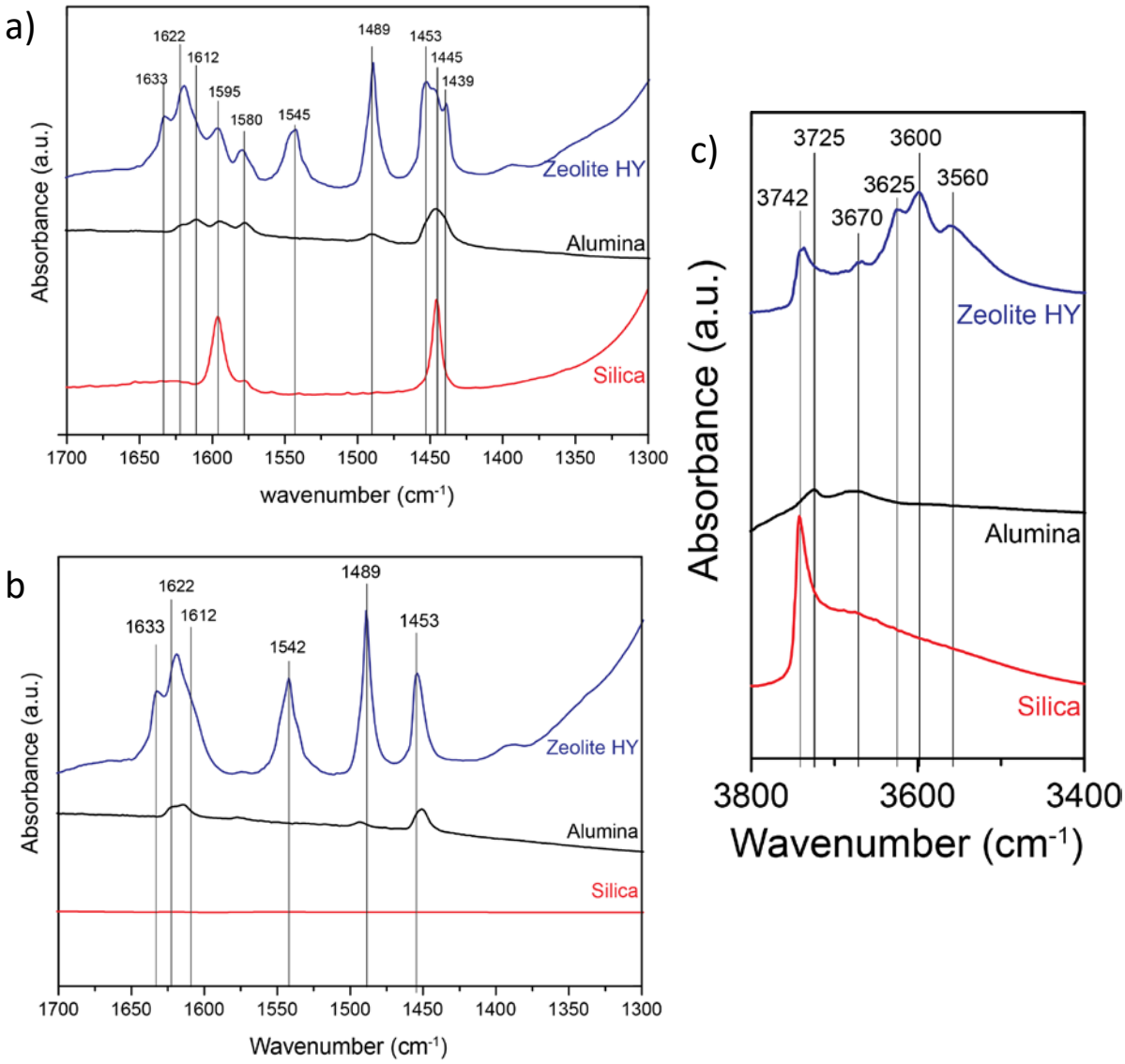

Figure S8: FT-IR spectra recorded after 30 minutes of pyridine adsorption (a) and after subsequent temperature programmed desorption at 200 °C under vacuum (b) for the three reference samples Zeolite H-Y (blue), Alumina (black), and Silica (red). The FT-IR spectrum recorded after sample activation is depicted in (c) with a zoom on the O-H vibrational region. All spectra are corrected for weight of the wafer and plotted with an offset for clarity.

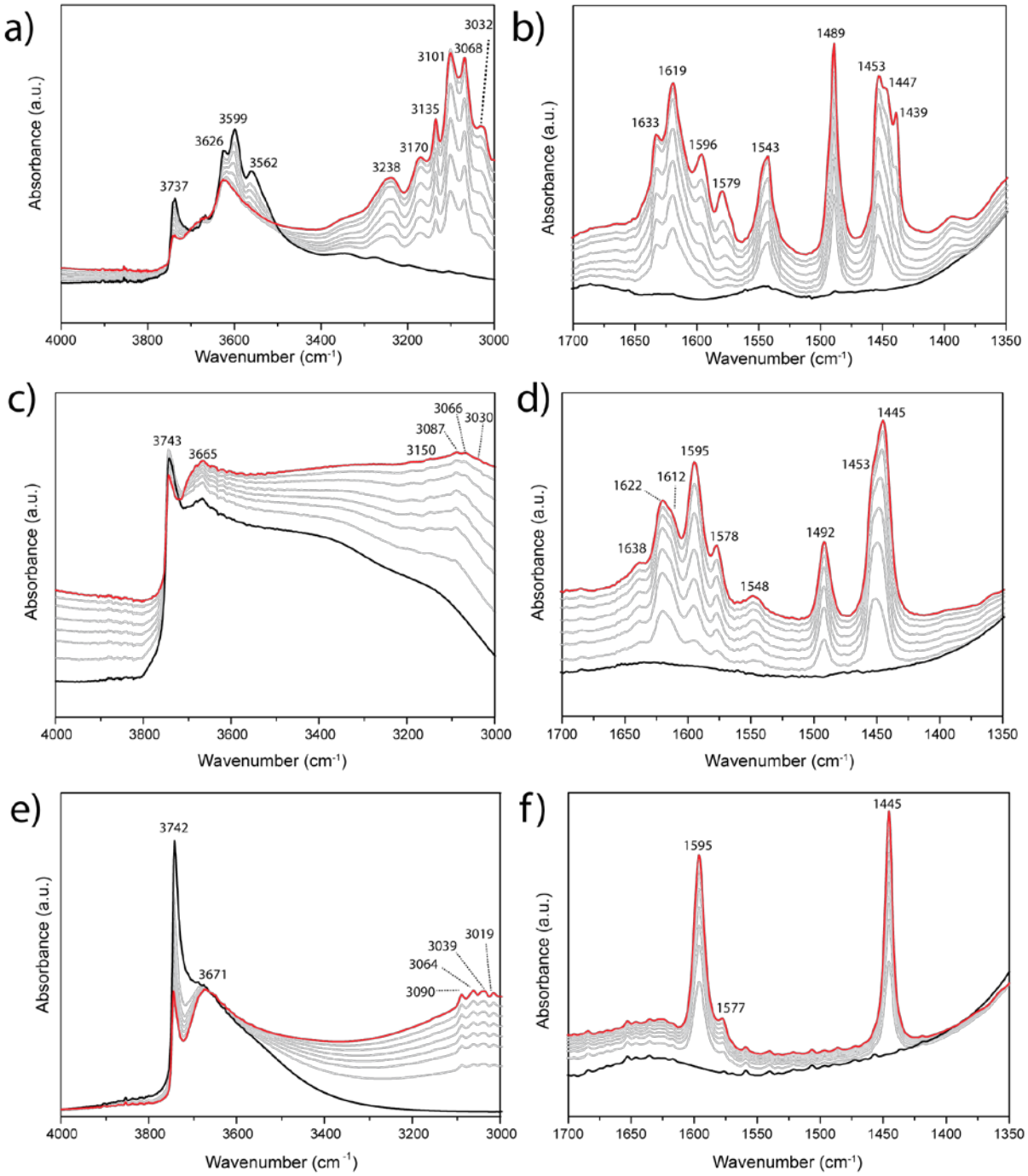

Figure S9: FT-IR spectra upon pyridine adsorption at room temperature for zeolite H-Y (a-b), alumina (c-d), and silica (e-f). Two regions of the spectra are represented: O-H stretching (left) and pyridine ring bending (right). The starting spectrum (t = 0 min) is shown in black, while the final spectrum (t = 30 min) is shown in red (sample at pyridine saturation at ca. 12 mbar).

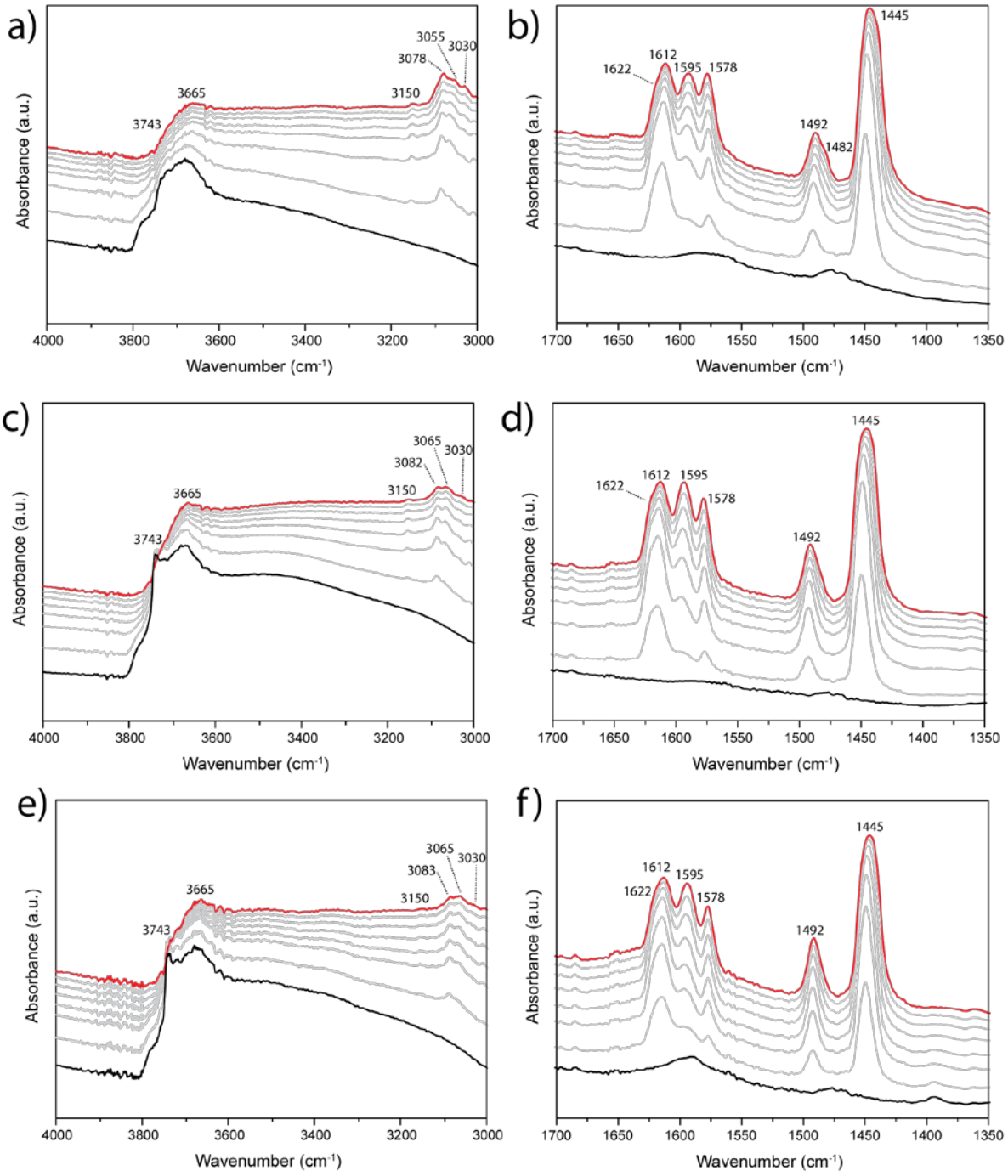

Figure S10: FT-IR spectra upon pyridine adsorption at room temperature for ASA-1 (a-b), ASA-5 (c-d), and ASA-10 (e-f). Two regions of the spectra are represented: O-H stretching (left) and pyridine ring bending (right). The starting spectrum (t = 0 min) is shown in black, while the final spectrum (t = 30 min) is shown in red (sample at pyridine saturation at ca. 12 mbar).

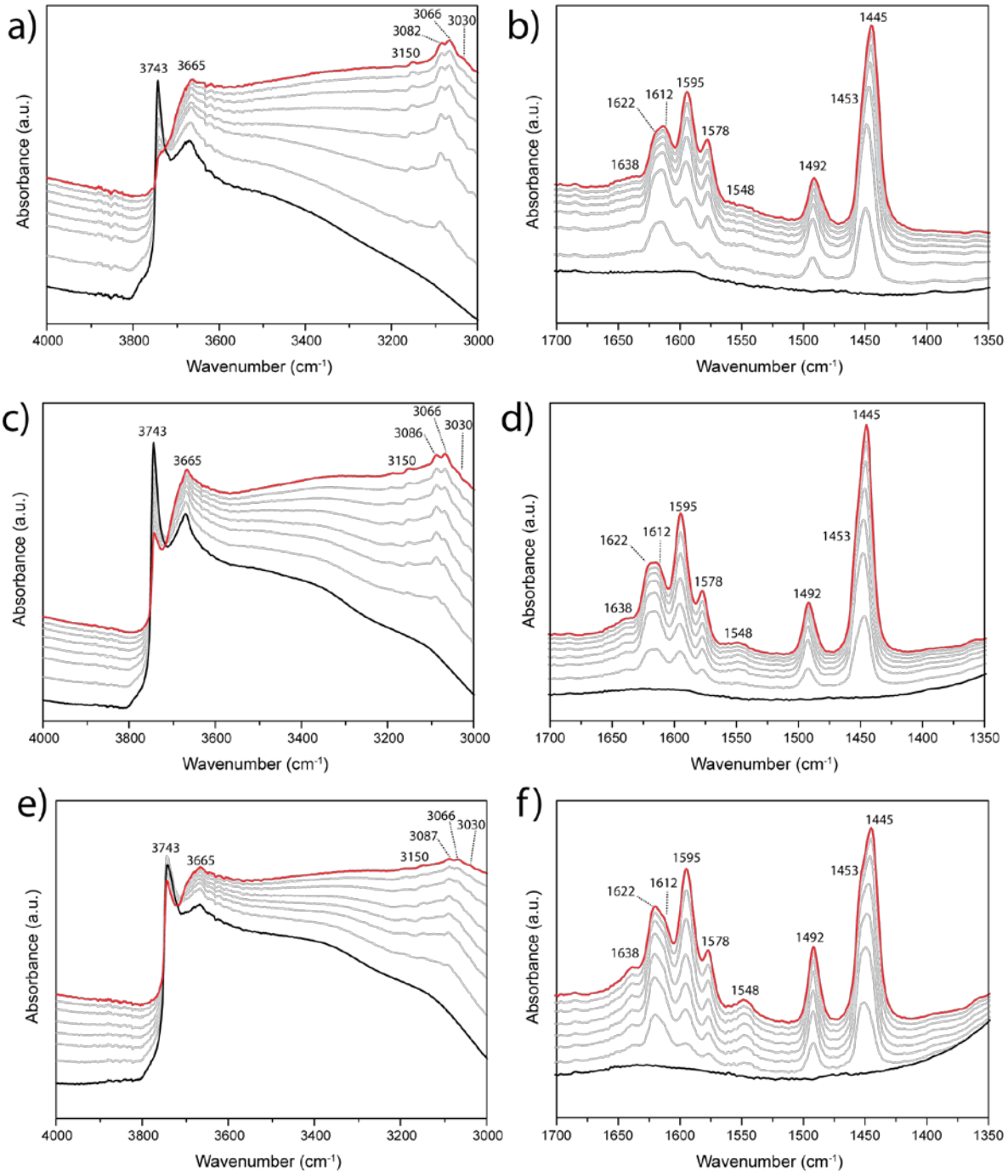

Figure S11: FT-IR spectra upon pyridine adsorption at room temperature for ASA-20 (a-b), ASA-30 (c-d), and ASA-40 (e-f). Two regions of the spectra are represented: O-H stretching (left) and pyridine ring bending (right). The starting spectrum (t = 0 min) is shown in black, while the final spectrum (t = 30 min) is shown in red (sample at pyridine saturation at ca. 12 mbar).

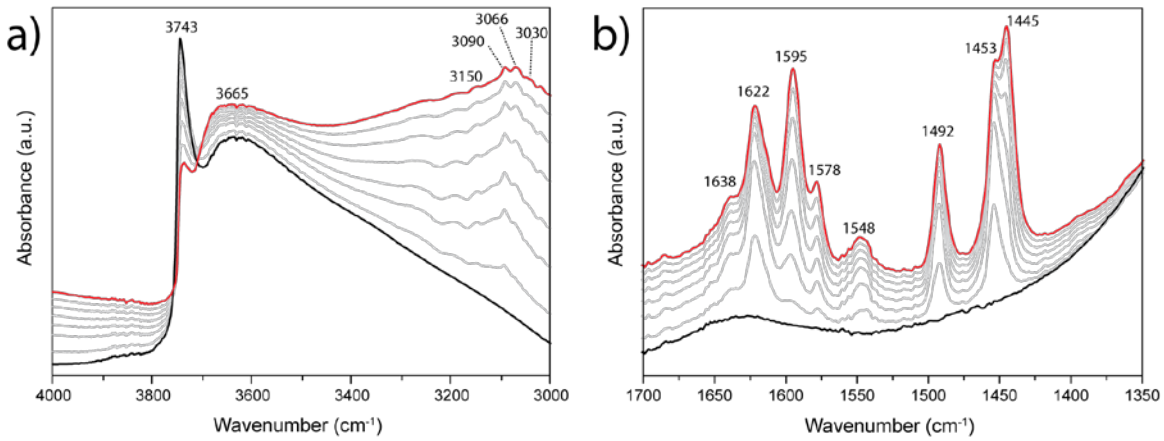

Figure S12: FT-IR spectra upon pyridine adsorption at room temperature for ASA-70). Two regions of the spectra are represented: O-H stretching (left) and pyridine ring bending (right). The starting spectrum (t = 0 min) is shown in black, while the final spectrum (t = 30 min) is shown in red (sample at pyridine saturation at ca. 12 mbar).

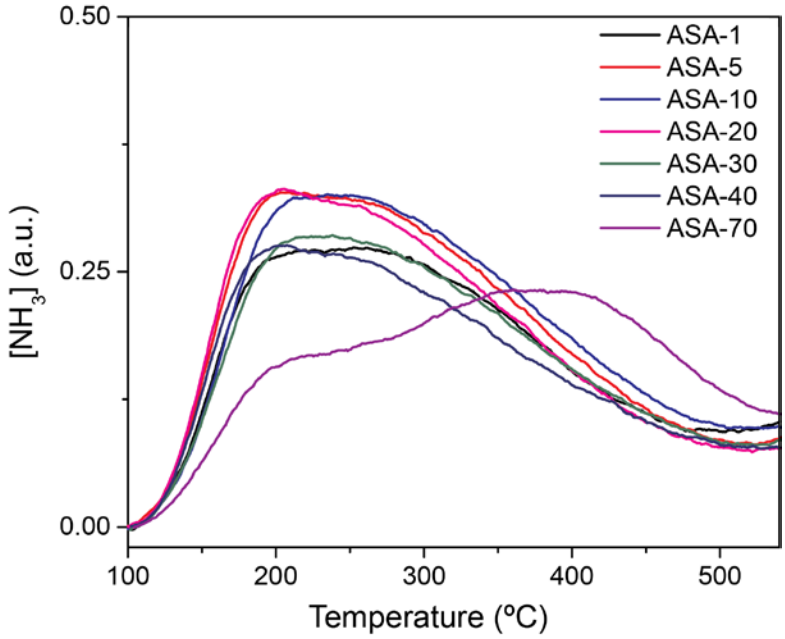

Figure S13: NH3-TPD profiles versus temperature for the seven ASA samples: ASA-1 (black), ASA-5 (red), ASA-10 (blue), ASA-20 (magenta), ASA-30 (green), ASA-40 (marine), and ASA-70 (purple).

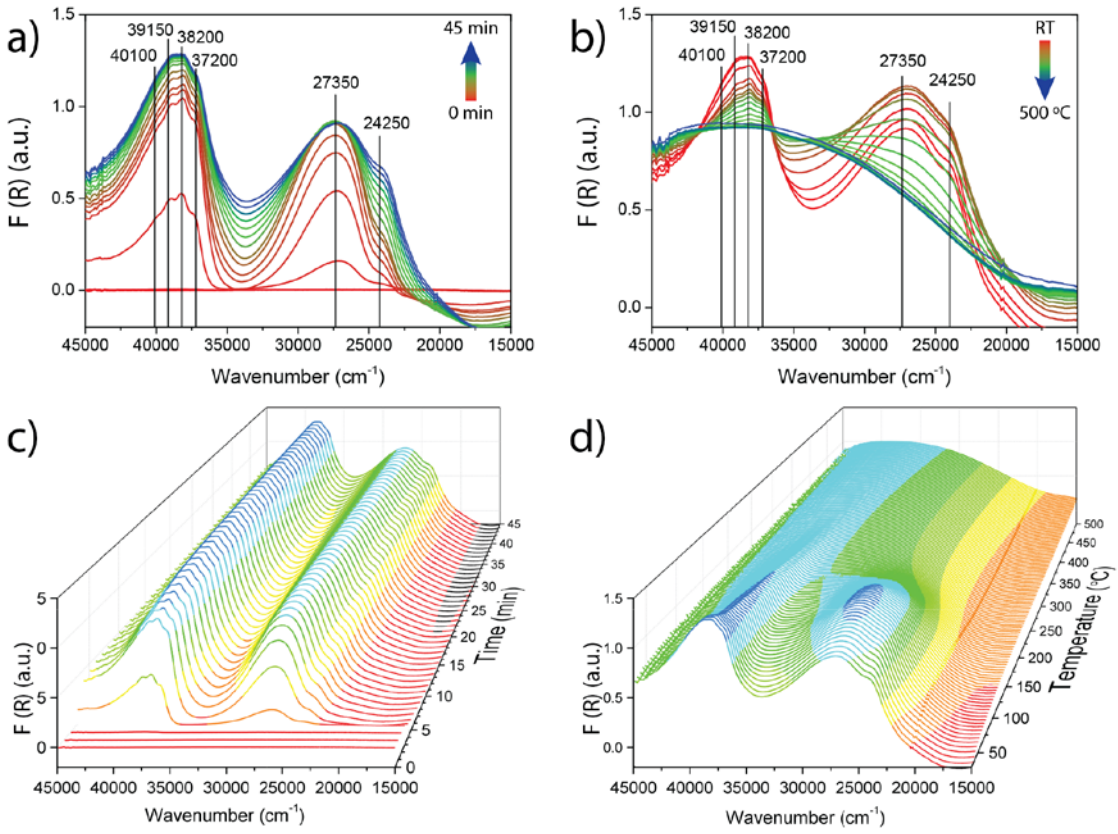

Figure S14: UV-Vis diffuse reflectance spectra of Silica taken during the adsorption of pyridine at RT (a) and the consecutive temperature-programmed desorption of pyridine. (b) The respective 3-D graphs are depicted below and illustrate the course of adsorption as a function of time (c) and the course of desorption as a function of temperature. (d)

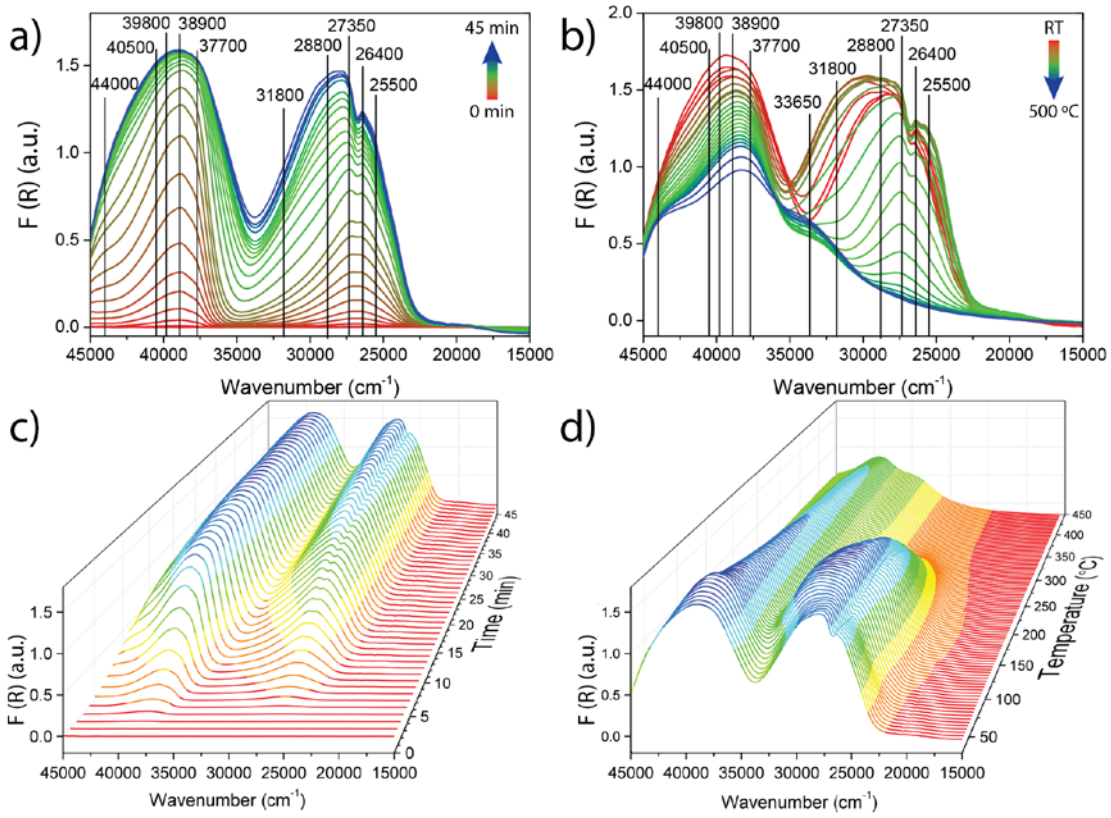

Figure S15: UV-Vis diffuse reflectance spectra of Alumina taken during the adsorption of pyridine at RT (a) and the consecutive temperature-programmed desorption of pyridine. (b) The respective 3-D graphs are depicted below and illustrate the course of adsorption as a function of time (c) and the course of desorption as a function of temperature. (d)

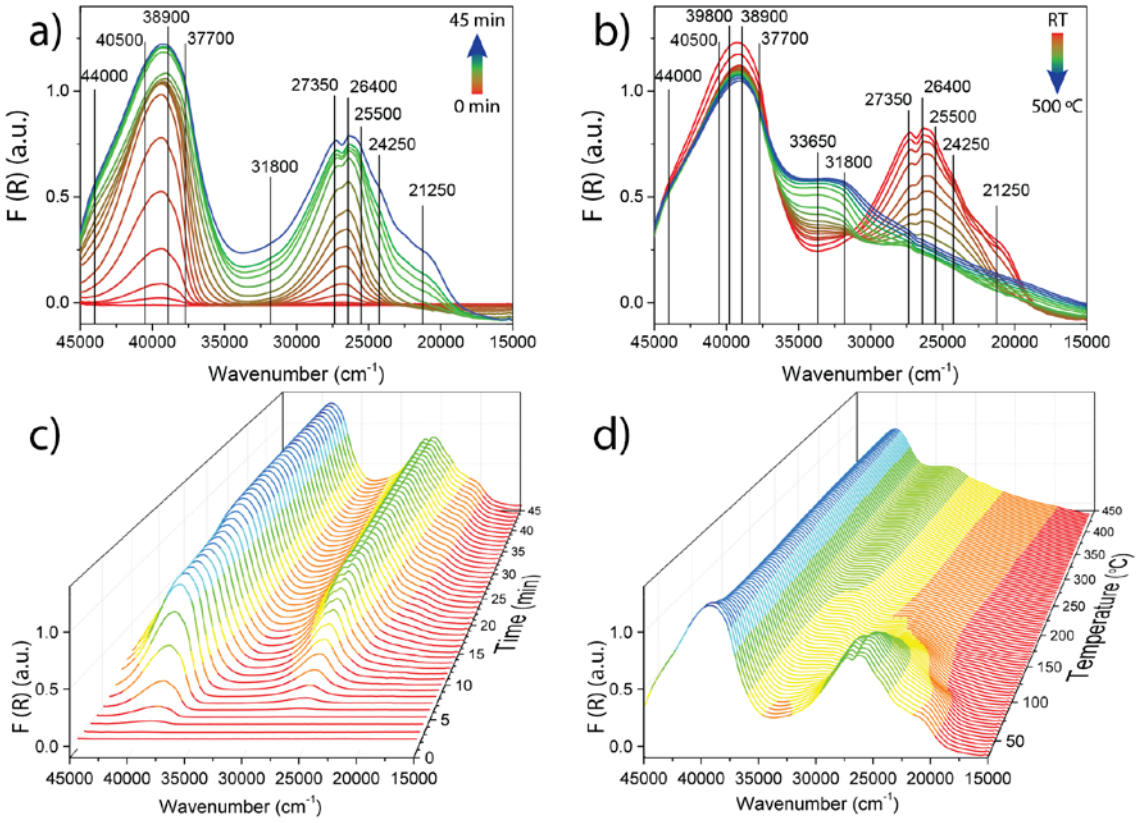

Figure S16: UV-Vis diffuse reflectance spectra of zeolite H-Y taken during the adsorption of pyridine at RT (a) and the consecutive temperature-programmed desorption of pyridine. (b) The respective 3-D graphs are depicted below and illustrate the course of adsorption as a function of time (c) and the course of desorption as a function of temperature. (d)

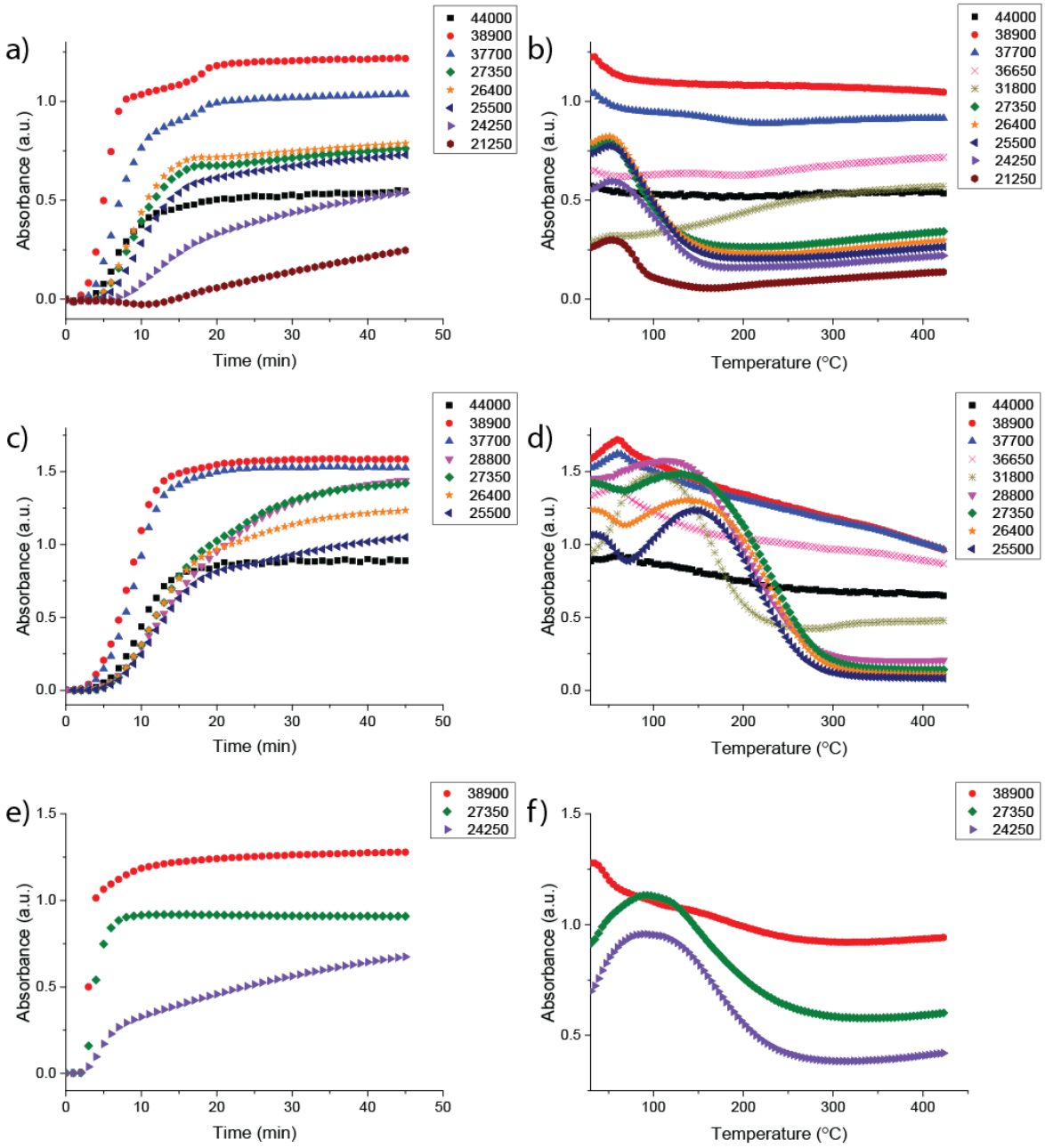

Figure S17: Evolution of the intensity of the absorption bands in the UV-Vis region during the respective adsorption (as a function of time) and desorption (as a function of temperature) of pyridine on the three reference samples Zeolite H-Y (a-b), Alumina (c-d), and Silica (e-f).

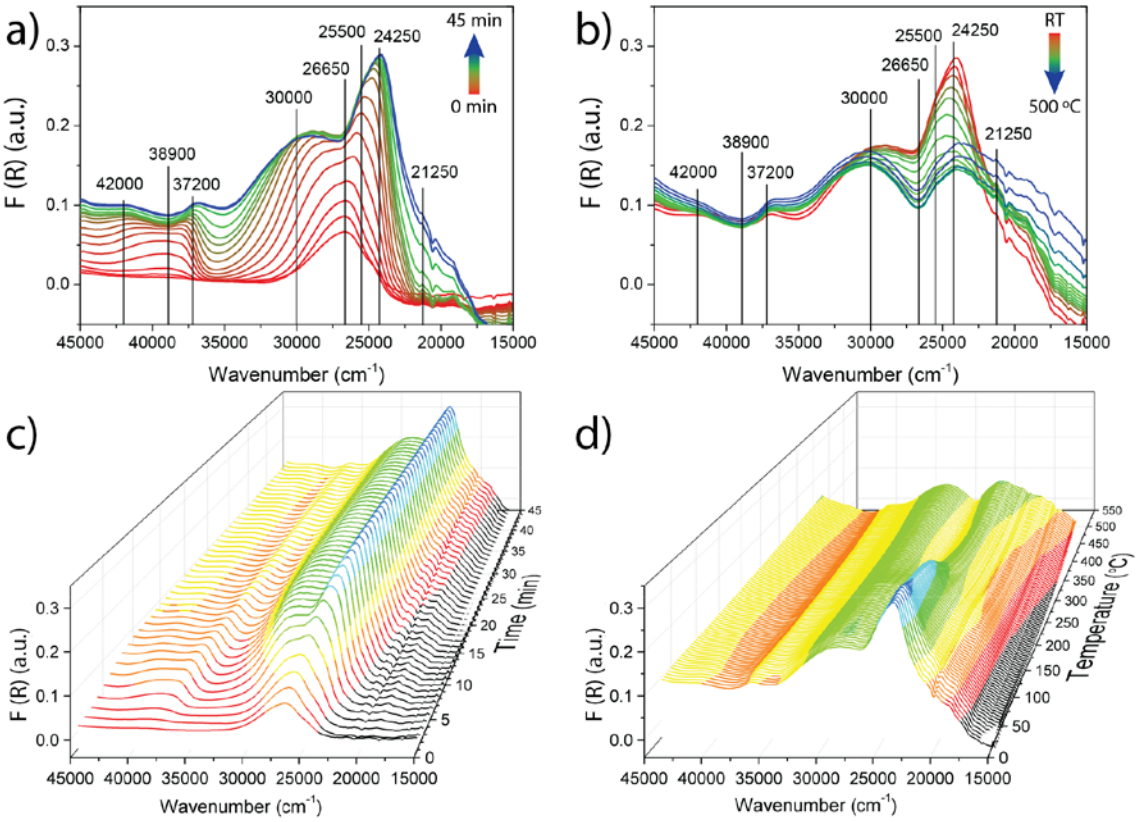

Figure S18: UV-Vis diffuse reflectance spectra of ASA-1 taken during the adsorption of pyridine at RT (a) and the consecutive temperature-programmed desorption of pyridine. (b) The respective 3-D graphs are depicted below and illustrate the course of adsorption as a function of time (c) and the course of desorption as a function of temperature. (d)

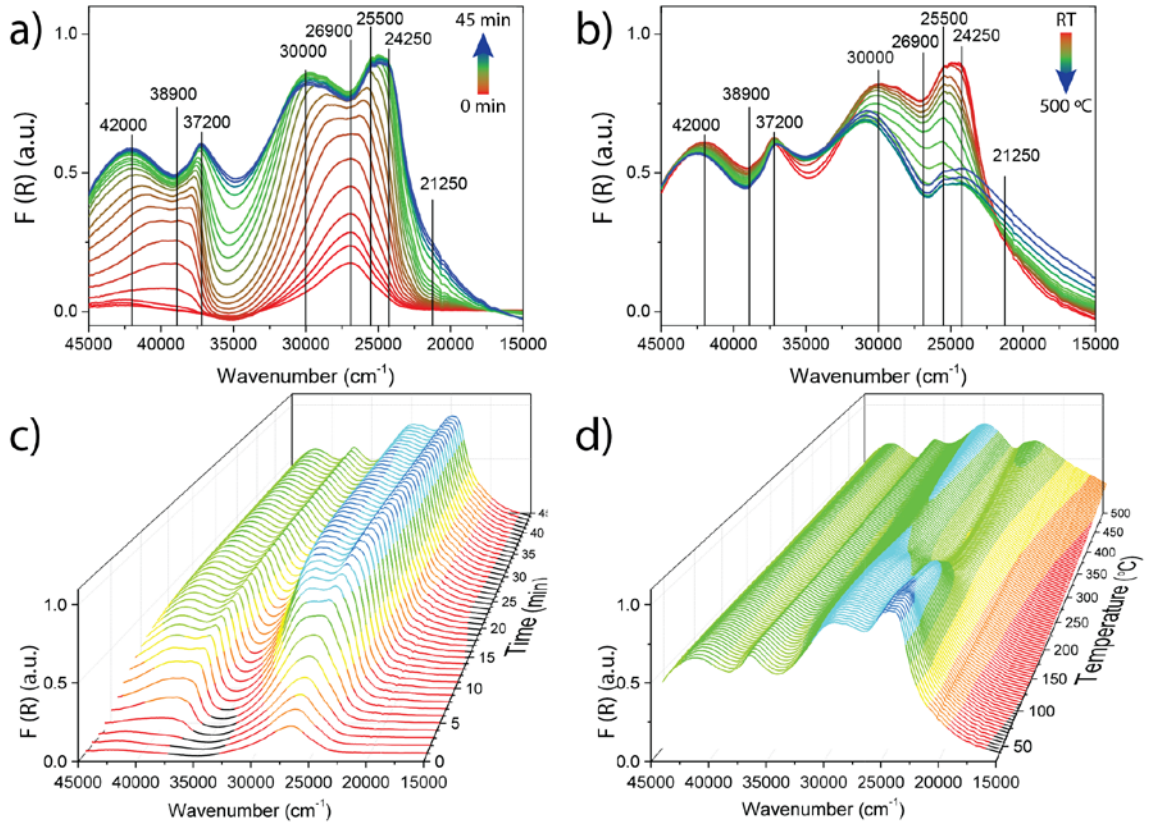

Figure S19: UV-Vis diffuse reflectance spectra of ASA-5 taken during the adsorption of pyridine at RT (a) and the consecutive temperature-programmed desorption of pyridine. (b) The respective 3-D graphs are depicted below and illustrate the course of adsorption as a function of time (c) and the course of desorption as a function of temperature. (d)

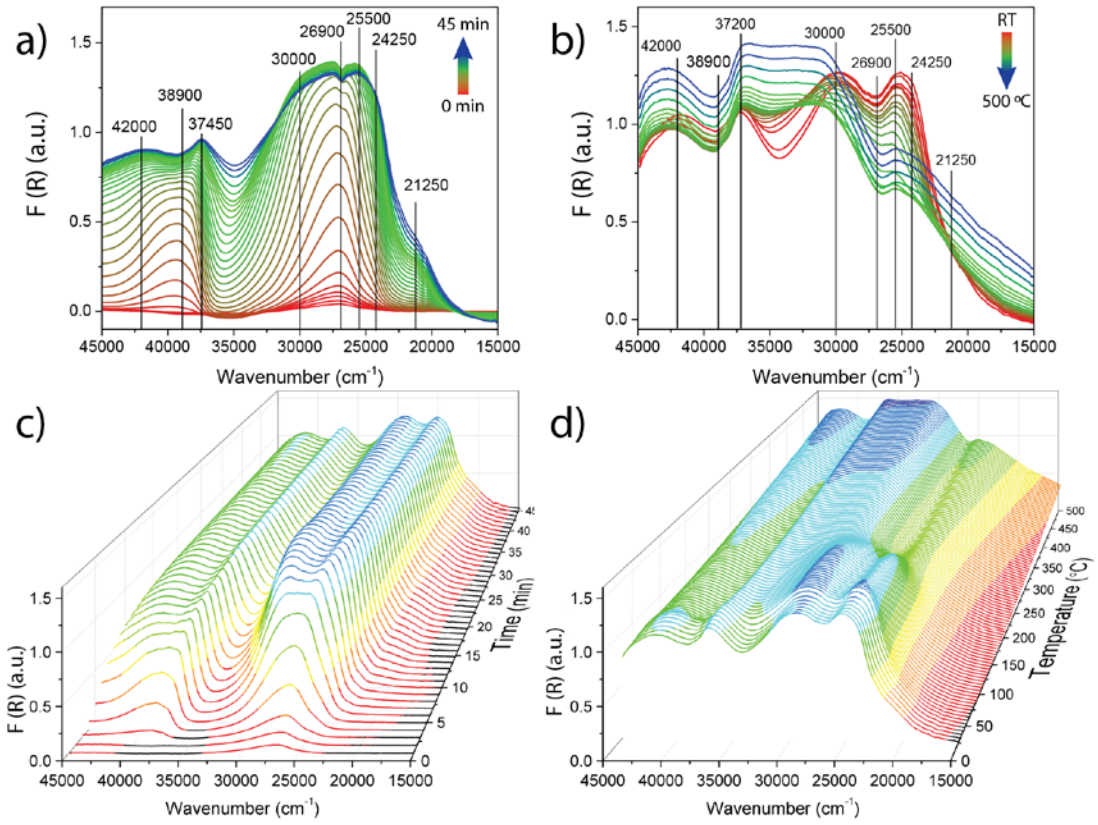

Figure S20: UV-Vis diffuse reflectance spectra of ASA-10 taken during the adsorption of pyridine at RT (a) and the consecutive temperature-programmed desorption of pyridine. (b) The respective 3-D graphs are depicted below and illustrate the course of adsorption as a function of time (c) and the course of desorption as a function of temperature. (d)

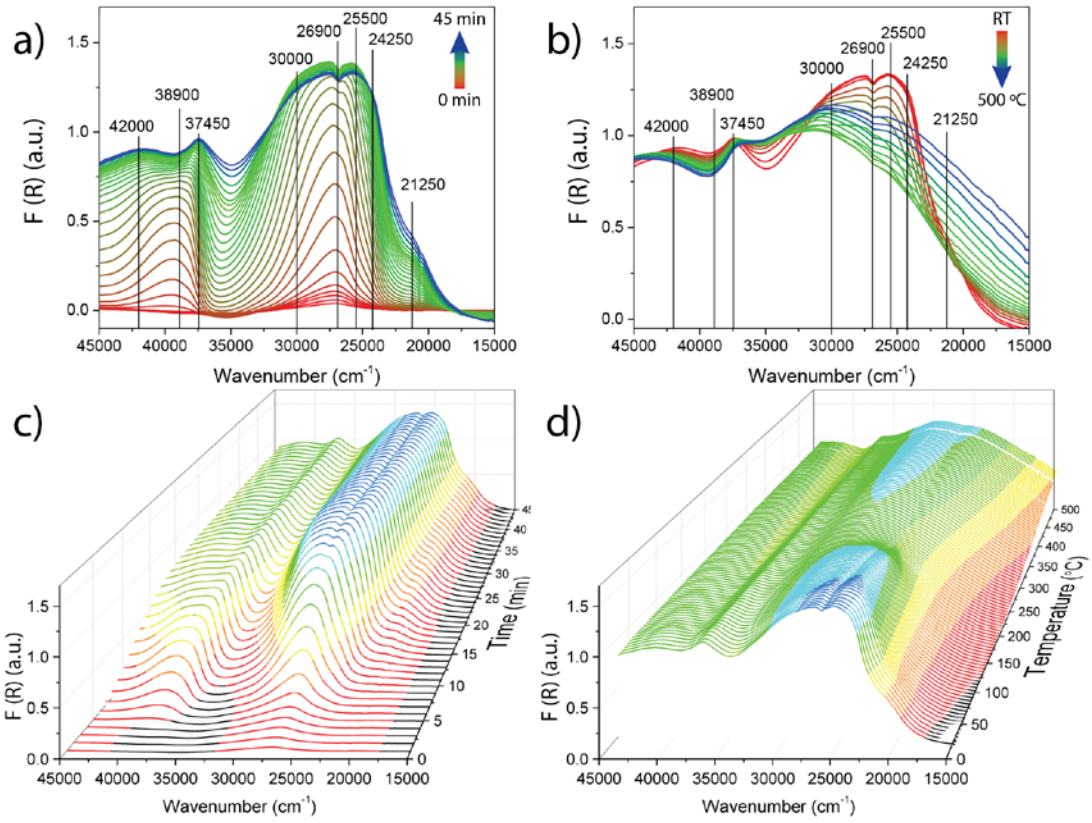

Figure S21: UV-Vis diffuse reflectance spectra of ASA-20 taken during the adsorption of pyridine at RT (a) and the consecutive temperature-programmed desorption of pyridine. (b) The respective 3-D graphs are depicted below and illustrate the course of adsorption as a function of time (c) and the course of desorption as a function of temperature. (d)

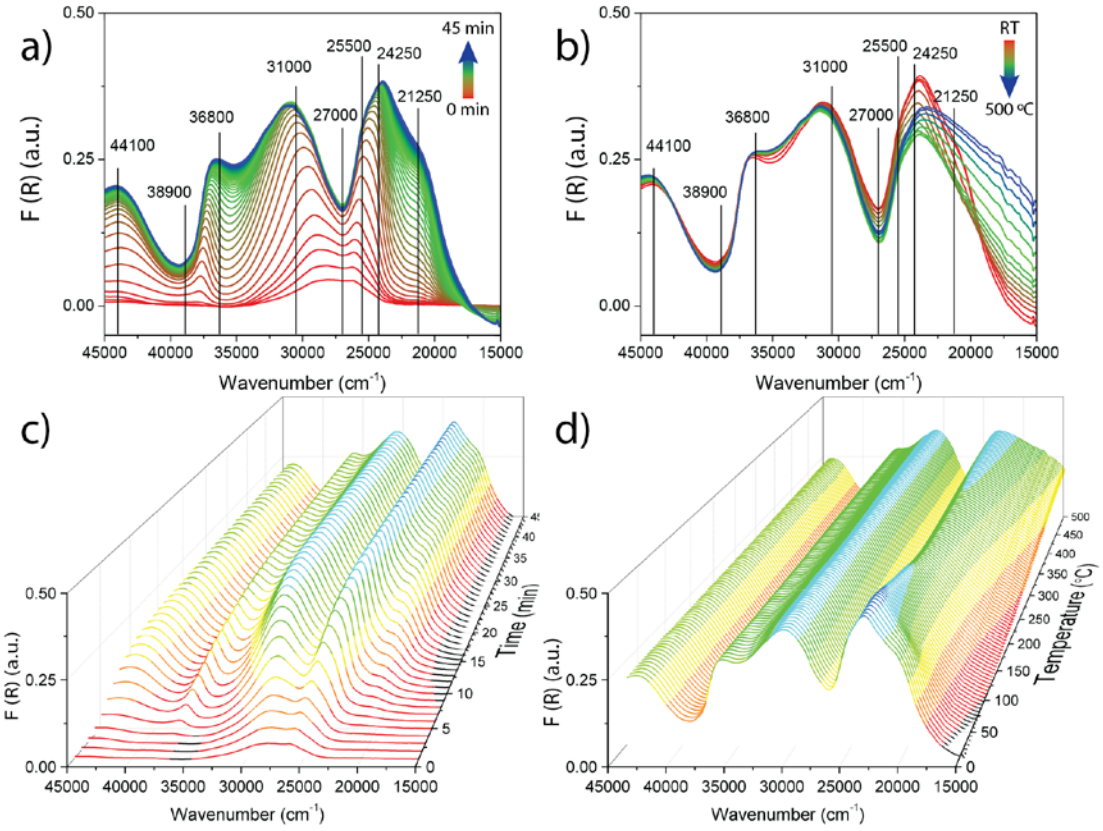

Figure S22: UV-Vis diffuse reflectance spectra of ASA-30 taken during the adsorption of pyridine at RT (a) and the consecutive temperature-programmed desorption of pyridine. (b) The respective 3-D graphs are depicted below and illustrate the course of adsorption as a function of time (c) and the course of desorption as a function of temperature. (d)

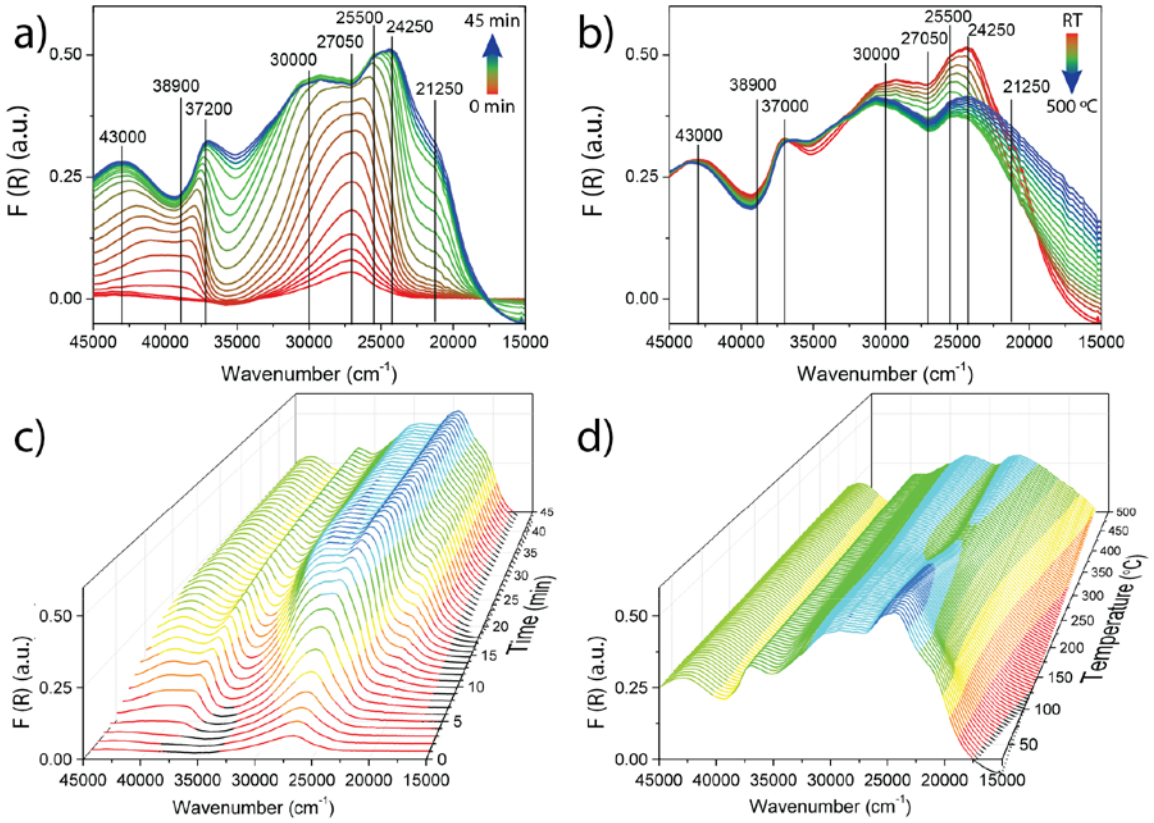

Figure S23: UV-Vis diffuse reflectance spectra of ASA-40 taken during the adsorption of pyridine at RT (a) and the consecutive temperature-programmed desorption of pyridine. (b) The respective 3-D graphs are depicted below and illustrate the course of adsorption as a function of time (c) and the course of desorption as a function of temperature. (d)

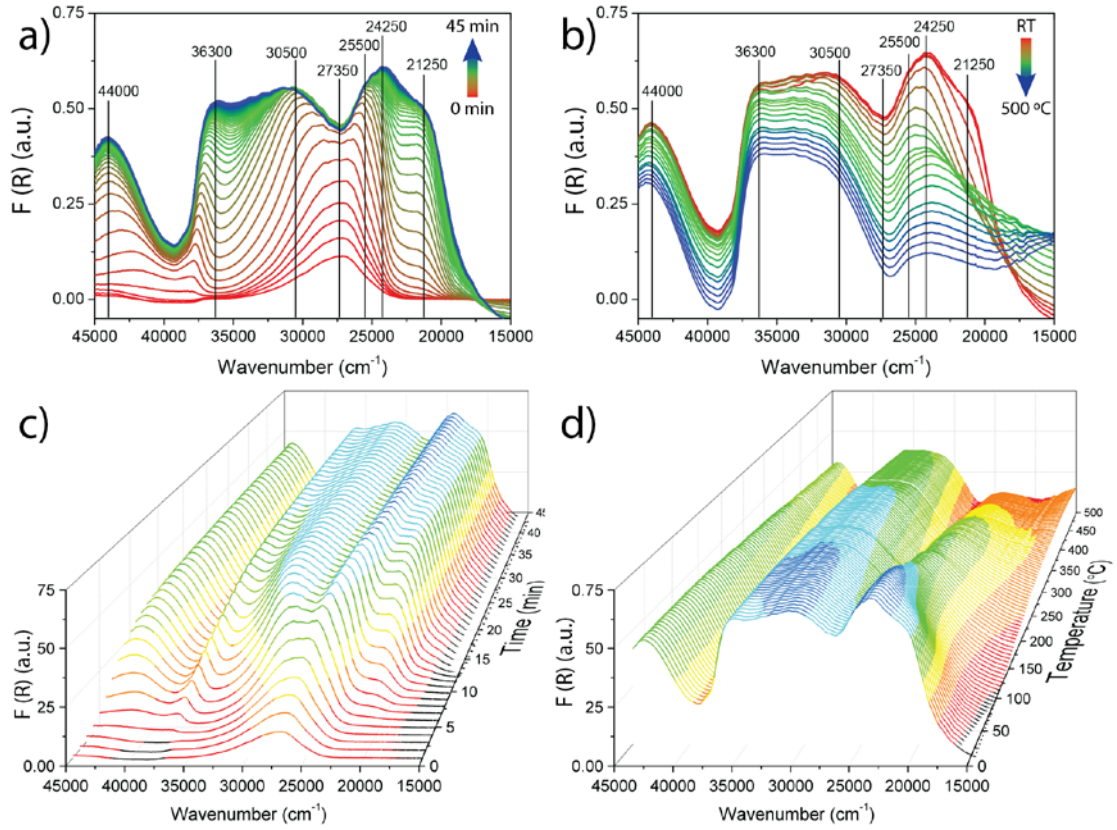

Figure S24: UV-Vis diffuse reflectance spectra of ASA-70 taken during the adsorption of pyridine at RT (a) and the consecutive temperature-programmed desorption of pyridine. (b) The respective 3-D graphs are depicted below and illustrate the course of adsorption as a function of time (c) and the course of desorption as a function of temperature. (d)

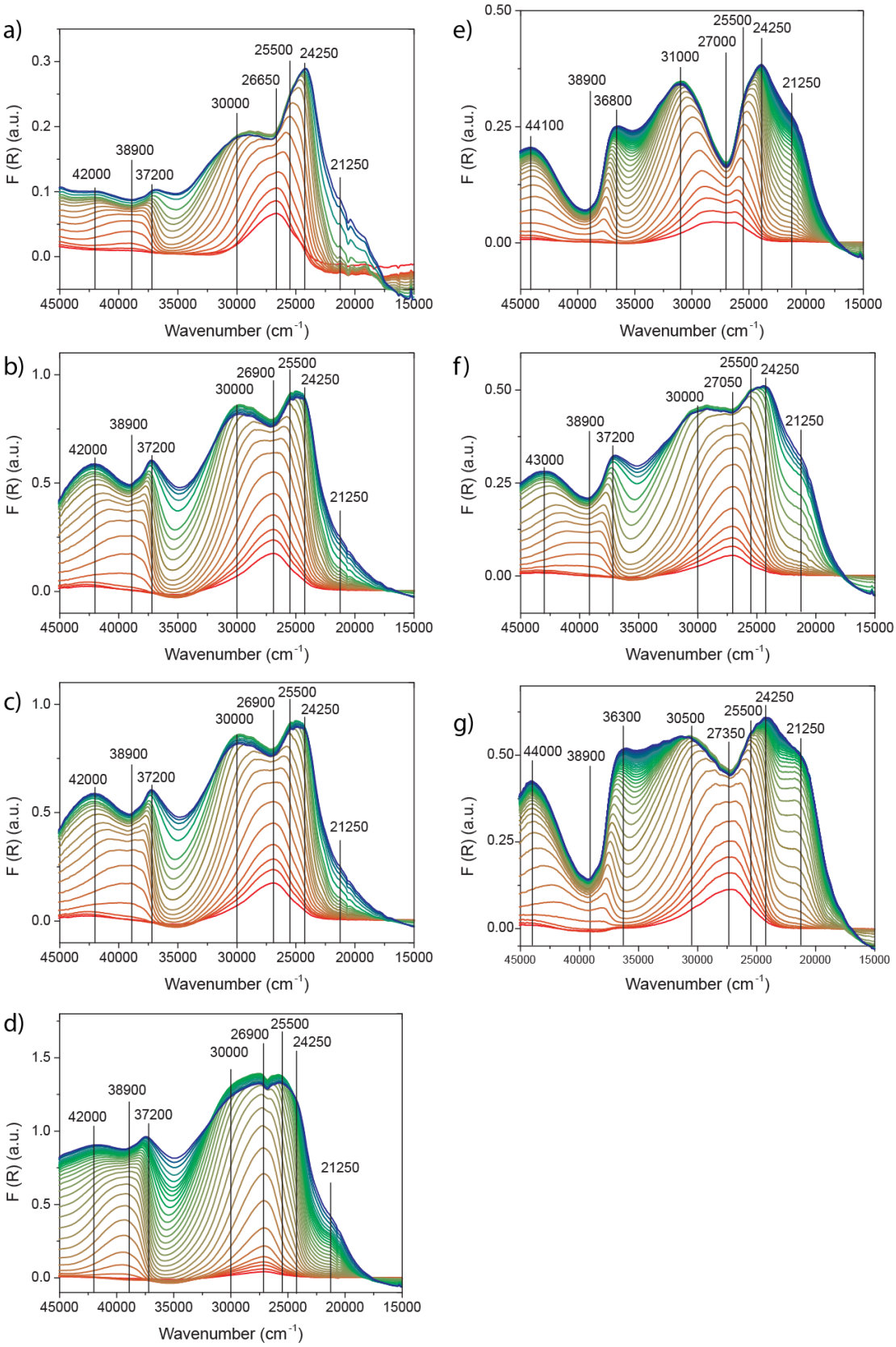

Figure S25: UV-Vis diffuse reflectance spectra of ASA-1 (a), ASA-5 (b), ASA-10 (c), ASA-20 (d), ASA-30 (e), ASA-40 (f), and ASA-70 (g), taken during the adsorption of pyridine at RT.